Redox-Induced Transitions in Bovine Cytochrome bc_1 Complex Studied by Perfusion-Induced ATR-FTIR Spectroscopy†

Masayo Iwaki,‡ Livia Giotta,‡ Akinyemi O. Akinsiku,‡ Hermann Schägger,§ Nicholas Fisher,‡ Jacques Breton,|| and Peter R. Rich*,‡

Glynn Laboratory of Bioenergetics, Department of Biology, University College London, Gower Street, London WC1E 6BT, U.K., Service de Bioénergétique, Bât. 532, CEA-Saclay, 91191 Gif-sur-Yvette Cedex, France, and Institut für Biochemie I, Universitätsklinikum Frankfurt, D-60590 Frankfurt am Main, Germany

Received February 24, 2003; Revised Manuscript Received July 25, 2003

ABSTRACT: Redox transitions in a film of detergent-purified bovine cytochrome bc_1 complex were investigated by perfusion-induced attenuated total reflection Fourier transform infrared (ATR-FTIR) spectroscopy. The technique provides a flexible method for generating redox-induced IR changes of components of bovine cytochrome bc_1 complex at a high signal:noise ratio. These IR redox difference spectra arise from perturbations of prosthetic groups and surrounding protein. Visible difference spectra were recorded synchronously using a light beam reflected from the exposed prism surface and provided a quantitative means of determining the redox transitions that were occurring. IR and visible redox difference spectra of iron−sulfur protein/cytochrome c_1, heme b_H, and heme b_L were separated by selective reduction and/or oxidation that extends published data on the homologous bacterial enzyme. Several bands could be tentatively assigned to redox-sensitive modes of hemes and ubiquinone and changes in the surrounding protein by comparison with available data for bacterial bc_1 complex, other related heme proteins, and model compounds. Some tentative assignments of further signals to specific amino acids are made on the basis of known crystal structures.

Bovine mitochondrial cytochrome bc_1 complex is a member of a superfamily of membrane-embedded enzymes that occur widely in eukaryotic and prokaryotic respiratory and photosynthetic electron transfer chains. Although the bovine enzyme is composed of 11 subunits (*1*), only three of these ["Rieske" iron−sulfur protein (ISP),[1] cytochrome c_1, and cytochrome *b*] are common to the superfamily. These three subunits contain the four redox-active prosthetic groups (a 2Fe-2S cluster, heme C, and two heme B forms, respectively) and form a core structure that catalyzes its ubiquinol-cytochrome *c* oxidoreductase and associated transmembrane proton transfer activities. Bacterial forms of the enzyme are composed of homologues of these three redox-active subunits, generally with a fourth small nonredox polypeptide (*2*). Functions of the additional subunits that are associated with mitochondrial bc_1 complexes are unclear, except for a processing protease activity of one or more of the large "core subunits" (*3*−*5*).

Structures of several eukaryotic *bc* complexes have been determined at atomic resolution (*6*−*9*). It is widely agreed (*10*) that the electron and proton transfer pathway occurs by a "Q-cycle" mechanism (*11*). Ubiquinol oxidation at the ubiquinol-binding "Q_o" site results in a concerted electron transfer in which the first electron is transferred to the ISP and the second to the lower-potential heme B, termed b_L. The electron on the ISP is passed *via* cytochrome c_1 to the substrate cytochrome *c*. The electron on heme b_L moves perpendicular to the membrane plane within the cytochrome *b* to reduce the higher-potential heme b_H. Reduced heme b_H reduces ubiquinone, which is bound at a second ubiquinone-binding site termed Q_i, first to a bound, stabilized semiquinone and then with a second electron to ubiquinol. The Q-cycle provides a very efficient means of utilizing the energy of electron transfer to form a proton-motive force across the membrane.

The thermodynamic properties of the prosthetic groups are known in some detail (Table 1) and, together with the structures of the proteins, are in accord with expectations from the Q-cycle mechanism. However, some key details about the basic electron and proton transfer mechanism remain unclear. Particularly enigmatic are the chemical and physical factors that cause the strict bifurcation of electron transfer at the Q_o site (*12*, *13*). For example, questions about whether a remarkable long-range rotation of the globular protein domain of the ISP center is an essential feature for bifurcated electron transfer remain (*14*−*16*). Furthermore, on the basis of positions of various bound inhibitors, the Q_o site appears to be rather extensive. Other data on the EPR

† This work was funded by grants from the Wellcome Trust (Grant 062827), The Royal Society (Is/ESEP/JP), and the French and British Councils (Franco British Alliance Joint Research Programme, Project PN 98.009).

* To whom correspondence should be addressed: Glynn Laboratory of Bioenergetics, Department of Biology, University College London, Gower Street, London WC1E 6BT, U.K. Telephone and fax: (+44) 020 7679 7746. E-mail: prr@ucl.ac.uk.

‡ University College London.

§ CEA-Saclay.

|| Universitätsklinikum Frankfurt.

[1] Abbreviations: (ATR-)FTIR, (attenuated total reflection-)Fourier transform infrared; ISP, Rieske iron−sulfur protein; PMS, phenazine methosulfate; FMN, flavin mononucleotide; *x*−/*x*, reduced *minus* oxidized difference spectrum of component *x*.

10.1021/bi0343020 CCC: $25.00
Published on Web 09/04/2003

Table 1: Redox and Absorption Properties of Redox Components of Bovine Cytochrome bc_1 Complex

	redox potential at pH 7.5 (mV vs SHE)	extinction coefficient $\Delta\epsilon$ (mM^{-1} cm^{-1})	wavelength (nm)
all components		39.6	562−575
heme c_1	242[a]	18.9[e]	553−575
ISP	280[b]	−	−
heme b_L	−50[c]	14.9	566−575
heme b_H	80[c]	25.9	562−575
ubiquinone bound in the Q_i site	110−145 (QH_2/Q)[d]	−	−
	20−70 ($Q^{\bullet-}$/Q)[d]		
	200−230 (QH_2/$Q^{\bullet-}$)[d]		

[a] Assumed to be the same as the pH 7 value of Rich (*63*). [b] Assumed to be the same as the pH 7.4 value of Trumpower (*64*). [c] From Rich et al. (*48*). [d] Derived from pH 7 data in ref *65* and approximating $\Delta E_m/\Delta pH = -120$ mV for $QH_2/Q^{\bullet-}$. [e] From King (*43*).

line shape of the ISP have indicated that two ubiquinones might be bound within the Q_o site (*17*), a suggestion supported by some inhibitor binding titrations (*18*) and more recently by NMR monitoring of ubiquinone displacement (*19*). These observations have led to proposals that two ubiquinols are required for functioning of the Q_o site (*20*) or that two sequential binding positions for ubiquinone species might be operative (*12*). Unfortunately, the Q_o site is unoccupied by quinone substrate in available crystal forms, so this question remains unresolved. For both the Q_o and Q_i sites, and for the redox prosthetic groups, very little is presently known about which groups within the protein are specifically responsible for the extensive redox-linked protonation changes that are integral to the catalytic cycle.

Fourier transform infrared (FTIR) spectroscopy has been used extensively to probe structural changes in individual cofactors and amino acids in proteins. The first such studies on redox-induced changes were achieved by light-induced perturbation of photosynthetic reaction centers (*21*, *22*). Introduction of spectroelectrochemical cells allowed application of FTIR spectroscopy to redox changes in cytochrome *c* (*23*). Such methods, together with induction of redox changes with photochemicals, have since been extended to cytochrome *c* oxidase (*24*−*29*), complex I (*30*), and other redox proteins (*31*), providing information about modes of ligand binding, amino acid and prosthetic group changes, and protonation changes within the protein. One transmission FTIR study of a bc_1 complex has appeared, in this case by application of thin layer spectroelectrochemistry to induce redox transitions in a bacterial bc_1 complex (*32*). An alternative to transmission FTIR methods is the technique attenuated total reflection (ATR)-FTIR spectroscopy (*33*, *34*) which allows measurement of FTIR changes in the sample while an aqueous solution is perfused over its surface (Figure 1, top panel). The ATR-FTIR method has already been applied to various proteins, including rhodopsin, bacteriorhodopsin (*35*), the nicotinic acetylcholine receptor (*36*), cytochrome oxidase (*37*−*39*), and reaction centers (*40*), and its flexibility extends the types of transitions that can be analyzed by FTIR spectroscopy. Here we describe the application of ATR-FTIR spectroscopy to the study of redox changes in thin layers of bovine cytochrome bc_1 complex that have been deposited on the surface of a silicon microprism. The results extend published data on the bacterial bc_1 complex (*32*) and are interpreted in light of crystallographic data and by comparison with available vibrational information about related proteins and model compounds.

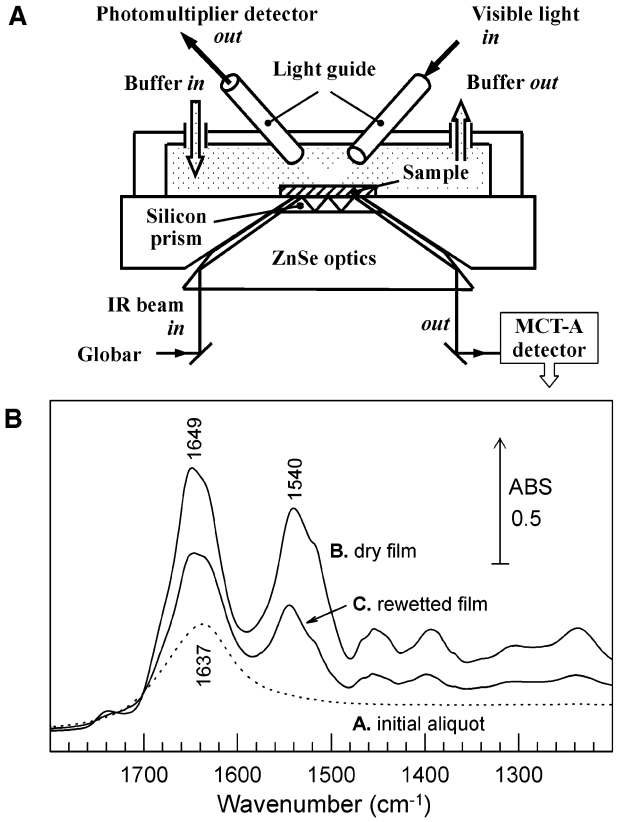

FIGURE 1: (A) ATR-FTIR/visible spectroscopy configuration and protein film preparation. The sample was deposited on the surface of a silicon microprism (3 mm diameter, three bounces, zinc selenide optics). The IR beam was reflected below the sample and detected by a liquid nitrogen-cooled MCT-A detector. A scanned visible beam from a 1 mm diameter fiber optic bundle was focused simultaneously through the protein sample, reflected from the top prism surface, and collected by a 3 mm fiber optic bundle for transfer to a photomultiplier detector. A small liquid chamber above the sample allowed continuous perfusion of buffers, which could be switched by computer-controlled valves. (B) ATR-FTIR absorption spectra of a sample of bovine cytochrome bc_1 complex during rehydrated film preparation. An 8 μL aliquot of 10 μM detergent-depleted protein suspended in 1 mM potassium phosphate buffer (pH 8.5) (see Materials and Methods) was placed on the silicon prism, and the absorption spectrum was recorded (trace A). The absorption spectrum was recorded again after the sample had been dried with nitrogen gas (trace B). Finally, the absorption spectrum was recorded again (trace C) after humidification for 30 min with saturated with water vapor, followed by full rehydration with 200 μL of 50 mM HEPES, 50 mM potassium phosphate, and 100 mM KCl (pH 7.5) for 60 min.

MATERIALS AND METHODS

Sample Preparation. Cytochrome bc_1 complex was isolated from beef heart Keilin-Hartree particles (*41*) by cholate solubilization and ammonium sulfate fractionation (*42*). The final preparation was redissolved to a final concentration of 100−300 μM in 20 mM sodium phosphate (pH 8) and stored in small aliquots at 77 K. Its concentration was estimated from an ascorbate-reduced *minus* ferricyanide-oxidized difference spectrum with an extinction coefficient of 18.9 mM^{-1} cm^{-1} for cytochrome c_1 at 553−575 nm (*43*). This preparation had a very low background succinate dehydrogenase

activity, which could be exploited for selective reduction of cytochrome b_H (see below) and retained close to one bound ubiquinone per bc_1 monomer as measured by quantitative ubiquinone extraction (*44*). So that the sample could adhere to the hydrophobic prism surface, excess detergent had to be removed. To achieve this, the sample was diluted 100-fold in 1 mM potassium phosphate buffer (pH 8.5) and pelleted by centrifugation at $100000g_{av}$ for 1 h. The precipitated pellet was homogenized into a small volume of 1 mM potassium phosphate (pH 8.5) to a final concentration of ~10 μM and stored at −80 °C until it was required. An 8 μL aliquot of the suspension was placed on the silicon ATR microprism and dried under a gentle stream of dry nitrogen. The protein film was humidified by exposure for 30 min to an atmosphere saturated with water vapor and then rehydrated by overlaying 200 μL of 50 mM *N*-(2-hydroxyethyl)piperazine-*N*′-2-ethanesulfonic acid (HEPES), 50 mM potassium phosphate, and 100 mM KCl at pH 7.5 for 60 min. Finally, a Perspex chamber, approximately 150 μL in volume, was placed over the sample to enable buffers to be passed over the exposed protein surface at a rate of approximately 1.5 mL/min. The perfusion buffer in all cases was 50 mM HEPES, 50 mM potassium phosphate, 100 mM KCl, and 5 μM phenazine methosulfate (PMS, a redox mediator) at pH 7.5. Various oxidants or reductants were added to this buffer to induce specific redox transitions (see below).

ATR-FTIR Measurements. IR spectra were recorded with a Nicolet Magna 860 or Bruker IFS 66S spectrometer equipped with a liquid nitrogen-cooled MCT-A detector and a 3 mm diameter three-reflection silicon ATR microprism (SensIR Europe). Measurements were taken at room temperature with a 2 mm aperture and a resolution of 4 cm^{-1}, and quoted frequencies have an accuracy of ± 1 cm^{-1}. ATR-FTIR difference spectra were recorded as redox changes were induced by the change of perfusant that was passed continuously above the surface of the film. Redox buffers were interchanged automatically using electronically controlled three-way valves. Buffer solutions were freshly prepared and degassed prior to the ATR-FTIR measurements, and those containing sodium dithionite were maintained under an argon atmosphere. Typically, a background spectrum was recorded during the flow of the first buffer over a period of approximately 40 s (an average of 64 interferograms for the Nicolet or 300 interferograms for the Bruker instrument). The flow was then switched to the second buffer, and a sample spectrum was recorded in the same way after a delay of 30 s for sample equilibration. The process was then reversed so that a full cycle resulted in both reduced *minus* oxidized and oxidized *minus* reduced difference spectra. The cycle was repeated automatically 30−60 times on the same sample, and data were averaged to provide a final spectrum.

For deuterium oxide (D_2O) exchange, sample preparation and ATR measurements were performed throughout by substitution of D_2O buffers at pD 7.5 and assuming pD is equal to the pH meter reading + 0.4 (*45*). The extent of H−D exchange was estimated using published methods that are based on the fact that the 60% N−H bending component of the amide II band (40% C−N stretch) shifts from 1545 to 1445 cm^{-1} on deuteration (*46*). Calculation based on this shift indicated that H−D exchange was >90% complete.

Where necessary, baseline corrections were made to allow for changes due to differences in perfusant constituents and for small changes in absolute spectra with some buffer pairs that arose from sample swelling and/or shrinkage and most likely caused predominantly by osmolarity differences. The correction for changes due to perfusion solutions was made by recording buffer changes in the absence of protein and subtraction from the experimental traces. Changes caused by protein swelling and/or shrinkage of the layer are composed of changes in the magnitude of the broad absolute spectra of protein and water and are essentially identical in shape to the difference spectrum of the fully rehydrated *versus* humidified film. Hence, this rehydration difference spectrum, suitably scaled down, was used qualitatively to correct for the small swelling and/or shrinkage changes that were sometimes present. In practice, such changes are anyway very broad in comparison to the much sharper redox-induced features and result only in a distortion of the underlying baseline in the amide I and II band regions without altering the frequencies of the redox-induced bands (e.g., see Figure 3).

Visible Difference Spectroscopy. Visible band difference spectra in the 510−584 nm range were recorded synchronously with the ATR-FTIR changes in an effort to quantify the redox transitions that were induced by the buffer changes. Light from a monochromator was delivered through the enzyme film, reflected from the upper prism surface, and delivered to a photomultiplier by fiber optics (Figure 1, top panel). Before a transition was initiated, the monochromator was stepped through the required range and I_o values were recorded. After making a transition, the monochromator was stepped again through the same range, and absorbance changes were computed as log I_o/I. Approximate absolute absorption spectra of the film could also be obtained by scanning an I_o spectrum before the film was deposited.

Light-Induced Transmission FTIR Measurements. For comparison of ATR-FTIR spectra with more conventional transmission methods, reduced *minus* oxidized difference spectra of intact detergent-dissolved cytochrome bc_1 complex (above) and of a soluble subfragment containing the globular domain of bovine cytochrome c_1 without any other redox prosthetic groups (prepared as described in ref *47*) were generated by photochemical reduction with FMN of samples mounted between CaF_2 windows (*26*). The samples were 4 nmol of cytochrome bc_1 complex, 200 μg of dodecyl maltoside, 0.2 nmol of FMN, and 8 nmol of potassium ferricyanide or 1.3 nmol of cytochrome c_1 subfragment (*47*), 1 nmol of FMN, and 2 nmol of potassium ferricyanide, in both cases in a final volume of 10 μL of 0.1 M Tricine buffer (pH 8.5). Background spectra of the oxidized samples were recorded, and samples were then illuminated with white light for 75 or 10 s, respectively (provided by a 100 W tungsten light projector and delivered to the sample by fiber optics), after which further spectra were recorded *versus* the oxidized backgrounds. Visible difference spectra (not shown) confirmed that the samples had changed from the fully oxidized to the fully reduced states.

RESULTS

IR Absorption Spectra during Preparation of the Protein Film. ATR-FTIR absorption spectra were measured at

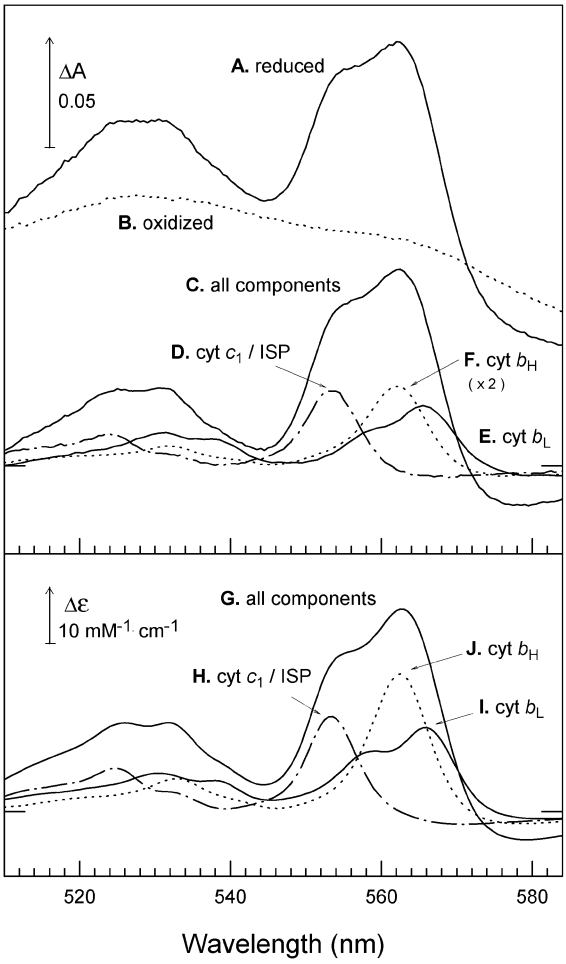

FIGURE 2: Perfusion-induced visible difference spectra of bovine cytochrome bc_1 complex. A rehydrated film prepared as described in the legend of Figure 1 was perfused with buffer [50 mM HEPES, 50 mM potassium phosphate, 100 mM KCl, and 5 μM PMS (pH 7.5)] containing 3 mM sodium dithionite and 3 mM KOH. After 30 s, an absolute reduced spectrum was recorded (trace A, average of five cycles) vs a baseline recorded in the absence of the protein film. The perfusant was switched to the same buffer containing 1 mM ferricyanide and 1 mM ferrocyanide, and an absolute oxidized spectrum (trace B, average of five cycles) was recorded after 30 s. The full reduced *minus* oxidized difference spectrum (trace C) was calculated as trace A *minus* trace B. Redox changes of individual components were achieved with specific pairs of perfusant buffers, as described in the text. The resulting reduced *minus* oxidized difference spectra (each an average of 10 transitions) are shown as follows: (trace D) cytochrome c_1 with ISP alone using hydroquinone/ferrocyanide and ferricyanide/ferrocyanide buffers, (trace E) heme b_L alone, using sodium dithionite and aerobic buffers, and (trace F, expanded 2-fold for clarity), heme b_H alone using succinate and fumarate/succinate buffers. The bottom panel shows the three component reference spectra of detergent-solubilized bovine cytochrome bc_1 complex in 50 mM HEPES, 50 mM potassium phosphate, 100 mM KCl, and 0.05% sodium cholate (pH 7.5) and obtained using conventional visible transmission spectroscopy and sequential reductants of 500 μM methylhydroquinone (which causes full reduction of cytochrome c_1 alone), 5 mM potassium succinate (which causes substantial reduction of heme b_H), and sodium dithionite (which reduces the remaining heme b_H and all heme b_L). The pure redox spectra [(trace H) c_1^-ISP$^-$/cyt c_1 ISP, (trace I) heme b_L^-/heme b_L, and (trace J) heme b_H^-/heme b_H] are normalized so that they represent the full extent of each component in the overall redox spectrum (trace G) and using assumptions that ϵ of cytochrome c_1 = 18.9 mM^{-1} cm^{-1} at 553−575 nm (*43*) and that the relative contributions of hemes b_H and b_L to the total heme B change at 562−575 nm are in a 0.7:0.3 ratio (*48*).

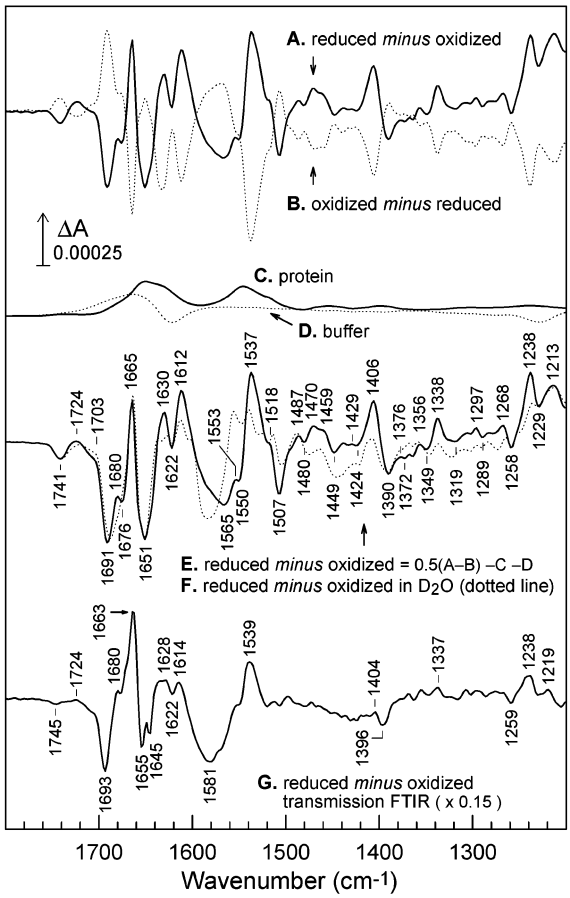

FIGURE 3: Perfusion-induced ATR-FTIR redox difference spectra of bovine cytochrome bc_1 complex. ATR-FTIR difference spectra were recorded synchronously under conditions used to generate the corresponding visible spectra in Figure 2. For each buffer change, a background spectrum was recorded (300 interferograms at 4 cm^{-1} resolution, data acquisition time of 40 s) followed by a sample spectrum at the appropriate time after the buffer had been switched. The spectra that are shown are averages of 30 reductive (trace A, solid line) and 30 oxidative (trace B, dotted line) transitions. Trace C shows the qualitatively assessed extent of baseline change in the reductive direction due to protein swelling and/or shrinkage, obtained by scaling down the absorption spectrum change that occurs during film preparation as the sample is hydrated (see Materials and Methods). Trace D shows the difference spectrum in the reductive direction due to buffer components alone (an average of 15 reductive traces and the inverse of 15 oxidative traces). The final reduced *minus* oxidized IR difference spectrum due solely to cytochrome bc_1 complex (trace E, solid line) was calculated as the average of trace A and inverse of trace B, *minus* the tow baseline correction traces C and D. An equivalent reduced *minus* oxidized IR difference spectrum in D_2O media after H−D exchange is overlaid (an average of 30 reductive traces and the inverse of 30 oxidative traces after baseline correction; trace F, dotted line). For comparison, trace G shows a reduced *minus* oxidized IR difference spectrum of cytochrome bc_1 complex, obtained by transmission FTIR spectroscopy using photochemical reduction of FMN to induce reduction (see Materials and Methods). Changes due to FMN have been subtracted, and the trace is a single measurement of 300 interferograms at 4 cm^{-1} resolution.

different stages during preparation of a rehydrated film of bovine cytochrome bc_1 complex (Figure 1, bottom panel). In the region of 1800−1200 cm^{-1}, the spectrum of the initial suspension of protein was essentially dominated by the O−H scissoring mode of water at 1637 cm^{-1} (trace A). After the compound had dried, the spectrum was dominated by the two main protein peaks at 1649 (amide I) and 1540 cm^{-1}

(amide II) together with some water that remained within the sample (trace B), presumably in the form of tightly bound structural water since further prolonged drying did not remove it. When the dried sample was humidified with saturated water vapor, the amplitude of the protein bands decreased and stabilized within 30 min at ~60% of the intensity of the dried sample. Finally, the protein film was rehydrated by overlaying a drop of 50 mM HEPES, 50 mM potassium phosphate, and 100 mM KCl at pH 7.5 (trace C). This caused a further slight decrease in the amplitude of the protein bands, which stabilized within 60 min. The humidification pretreatment produced a more stable protein film than one rewetted with buffer directly from the dry state.

Perfusion-Induced Visible Difference Spectra of Cyt bc_1 Complex. Perfusion-induced visible difference spectra of redox transitions induced in the protein film are shown in Figure 2. For full reduction and oxidation of the complex, the perfusant was alternated between buffer containing either 3 mM sodium dithionite and 3 mM KOH or 1 mM ferricyanide and 1 mM ferrocyanide. The KOH was added to minimize swelling and/or shrinkage changes by minimizing pH differences. Absolute absorption spectra in reduced and oxidized states (*vs* an I_o spectrum of the clean prism surface) were recorded 30 s after buffer exchange. The redox cycle was repeated five times, and the spectra were averaged to produce the traces shown in panels A and B of Figure 2. These absolute spectra showed that the protein film was undergoing full oxidation and reduction in response to buffer changes. The reduced *minus* oxidized difference spectrum (trace A *minus* trace B) is shown as trace C. At the end of experiments, reduced *minus* oxidized difference spectra were routinely re-recorded to check for sample stability. In all cases, no significant change in the extent or shape of spectra occurred, indicating that no denaturation or cofactor loss had occurred during the course of the measurements. Figure 2D shows the redox transition that occurred when the buffer was alternated between one containing 100 μM hydroquinone and 2 mM ferrocyanide and a second containing 1 mM ferricyanide and 1 mM ferrocyanide. Spectra were recorded 30 s after buffer exchange, and the spectrum that is shown is an average of five reductive spectra and the reverse of five oxidative spectra. The magnitudes and shapes of the positive peaks at 553 and 524 nm demonstrated that cytochrome c_1 and, therefore, the roughly isopotential ISP were undergoing oxidation or reduction, whereas both heme B forms remained unchanged.

For measurement of the redox transition of cyt b_L alone, a background was recorded after perfusion for 2 min with 3 mM sodium dithionite in buffer to cause full reduction of all redox components. The buffer was then replaced with an aerobic one without dithionite, and after 5 s, the difference spectrum was measured. The sample was reperfused with dithionite-containing buffer, and the measurement was repeated. The trace shown in Figure 2E is the inverse of an average of seven such oxidative spectra. The peaks at 565.5 and 531 nm and shoulders at 559 and 531 nm indicate that only the lower-potential heme b_L changed redox state during this treatment with no contribution from redox changes of other components.

Figure 2F shows the visible difference spectrum induced by alternation of buffer containing 300 μM succinate or 285 μM fumarate and 15 μM succinate. Spectra were recorded 30 s after buffer exchange, and the spectrum that is shown is an average of five reductive spectra and the reverse of five oxidative spectra. The spectrum exhibited positive peaks at 562 and 532 nm, and their shapes confirmed that only the heme b_H (and, presumably, the optically invisible Q_i site ubiquinone) redox state changed during this treatment.

Also shown in Figure 2 are quantitative reduced *minus* oxidized reference spectra of the three heme components (traces H−J) that make up the full redox difference spectrum (trace G). These were obtained with an identical bc_1 complex sample by conventional visible spectrometric methods. Comparison of the experimental traces (C−F) with these reference data indicates that the extents of redox changes of hemes c_1, b_H, and b_L under the selective partial reduction conditions of the ATR-FTIR experiments were 75, 30, and 70%, respectively, of their extents in the full redox difference spectra and also that each of these specific partial redox transitions had negligible contributions from redox transitions of the other hemes.

ATR-FTIR Redox Difference Spectra of the Whole Complex. Redox-induced ATR-FTIR difference spectra were recorded concurrently with the visible difference spectra shown in Figure 2, although more cycles were averaged to produce an adequate signal:noise ratio. Figure 3 shows the corresponding IR difference spectra resulting from full reduction and reoxidation of the bc_1 complex of the sample used for traces A and B in Figure 2. The raw data for an average of 30 cycles are shown for both reductive (trace A) and oxidative (trace B) directions. These spectra are nearly mirror images of each other, confirming the reversibility of the transitions. Adjustments were made to these spectra to minimize any baseline distortions due to protein swelling and/or shrinkage and buffer components. The estimated swelling and/or shrinkage spectrum that was subtracted is shown as trace C, and the spectrum due to change from oxidative to reductive buffer in the absence of protein is shown as trace D. To generate the final corrected reduced *minus* oxidized spectrum shown as trace E, the oxidized *minus* reduced spectrum (trace B) was inverted and averaged with the reduced *minus* oxidized one (trace A), and both the swelling and/or shrinkage (trace C) and the buffer (trace D) spectra were subtracted from it. The resultant reduced *minus* oxidized difference spectrum (trace E) exhibits principle features at 1741 (−), 1724 (+), 1691 (−), 1665 (+), 1651 (−), 1630 (+), 1622 (−), 1612 (+), 1565 (−), 1550 (−), 1537 (+), 1507 (−), 1406 (+), 1390 (−), 1338 (+), 1258 (−), 1238 (+), and 1213 (+) cm^{-1}.

Superimposed on the reduced *minus* oxidized spectrum in H_2O media (trace E) is an equivalent spectrum recorded in D_2O media after H−D exchange (trace F) and normalized so that the amide I changes are comparable. Differences between these two spectra can aid band assignments as described in detail below.

Figure 3 also shows for comparison (trace G) a reduced *minus* oxidized difference spectrum recorded by transmission FTIR spectroscopy of a sample of bc_1 complex in which full reduction was induced by photochemical reduction with FMN (see Materials and Methods). Although the complex exhibit much poorer signal:noise ratios because it could not be easily cycled repetitively, the principle features are consistent with the ATR-FTIR spectrum, but with the ATR-FTIR spectrum showing the expected increase in the relative

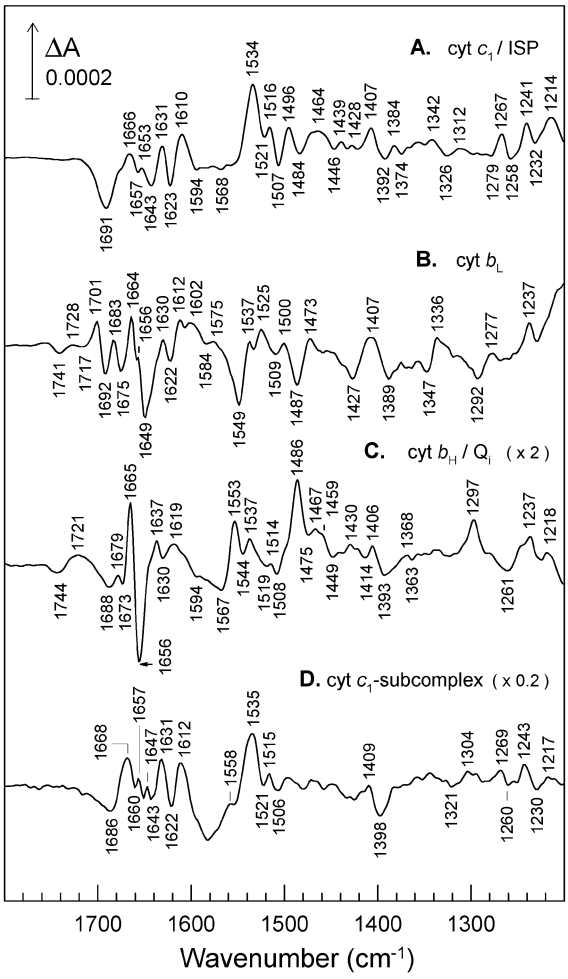

FIGURE 4: Perfusion-induced ATR-FTIR redox difference spectra of individual components of bovine cytochrome bc_1 complex. ATR-FTIR difference spectra were recorded synchronously under conditions used to initiate redox changes of specific components shown in traces D−F of Figure 2. For each buffer change, a background spectrum was recorded followed by a sample spectrum at the appropriate time after the buffer had been switched. Trace A is a redox difference spectrum of cyt c_1^-ISP$^-$/cyt c_1 ISP (average of 60 reductive and 60 oxidative spectra, 300 interferograms/spectrum), trace B a redox difference spectrum of heme b_L^-/heme b_L (average of 60 oxidative spectra, 64 interferograms/spectrum), trace C a redox difference spectrum of heme b_H^-/heme b_H (average of 60 reductive and 60 oxidative spectra, 300 interferograms/spectrum), and trace D a redox difference spectrum of pure cyt c_1^-/cyt c_1 in a soluble cytochrome c_1 subcomplex, obtained by transmission FTIR spectroscopy and with reduction induced by FMN-mediated photoreduction (see Materials and Methods; average of two samples, each of 300 interferograms at 4 cm^{-1} resolution). Where required, baseline corrections for swelling and/or shrinkage and/or buffer components were made as described in the legend of Figure 3.

signal intensity with decreasing frequency because of the increased depth of penetration of the evanescent wave (*33*).

ATR-FTIR Redox Difference Spectra of Cytochrome c_1 and ISP. The reduced *minus* oxidized IR difference spectrum due to cytochrome c_1 with ISP was recorded for the same samples used to generate the cytochrome c_1 visible redox spectrum in Figure 2D. The resultant spectrum, after correction for buffer reagents and swelling and/or shrinkage, is shown in Figure 4A and is an average of 60 reductive and the reverse of 60 oxidative spectra. It exhibits major bands at 1691 (−), 1666 (+), 1657 (−), 1653 (+), 1643 (−), 1631 (+), 1623 (−), 1610 (+), 1594 (−), 1534 (+), 1521 (−), 1516 (+), 1507 (−), 1496 (+), 1484 (−), 1464 (+), 1446 (−), 1439 (+), 1407 (+), 1392 (−), 1384 (+), 1342 (+), 1326 (−), 1312 (+), 1279 (−), 1267 (+), 1258 (−), 1241 (+), 1232 (−), and 1214 (+) cm^{-1}.

ATR-FTIR Redox Difference Spectra of Heme b_L. The reduced *minus* oxidized IR difference spectrum due to heme b_L was recorded for the same samples used to generate the heme b_L visible spectrum in Figure 2E. The resultant spectrum is plotted in Figure 4B as a reduced *minus* oxidized difference spectrum after correction for buffer reagents and swelling and/or shrinkage and is an average of 60 cycles. It exhibits major bands at 1741 (−), 1728 (+), 1717 (−), 1701 (+), 1692 (−), 1683 (+), 1675 (−), 1664 (+), 1649 (−), 1612 (+), 1602 (+), 1549 (−), 1537 (+), 1525 (+), 1509 (−), 1500 (+), 1487 (−), 1473 (+), 1427 (−), 1407 (+), 1389 (−), 1347 (−), 1336 (+), 1292 (−), 1277 (+), and 1237 (+) cm^{-1}.

ATR-FTIR Redox Difference Spectra of Heme b_H and Q_i Ubiquinone. The reduced *minus* oxidized IR difference spectrum due to heme b_H was recorded for the same samples used to generate the heme b_H visible spectrum in Figure 2F. Since the redox potentials of heme b_H and ubiquinone bound in the Q_i site overlap at this pH (ref *48* and Table 1), the spectrum will also contain ubiquinone contributions. The resultant spectrum, after correction for buffer reagents and swelling and/or shrinkage, is shown in Figure 4C and is an average of 60 reductive and the reverse of 60 oxidative spectra. This reduced *minus* oxidized difference spectrum exhibits major bands at 1744 (−), 1721 (+), 1688 (−), 1679 (+), 1673 (−), 1665 (+), 1656 (−), 1637 (+), 1630 (−), 1619 (+), 1567 (−), 1553 (+), 1544 (−), 1537 (+), 1519 (−), 1514 (+), 1508 (−), 1486 (+), 1475 (−), 1467 (+), 1459 (+), 1449 (−), 1430 (+), 1414 (−), 1406 (+), 1393 (−), 1368 (+), 1363 (−), 1297 (+), 1261 (−), 1237 (+), and 1218 (+) cm^{-1}.

DISCUSSION

Perfusion-induced ATR-FTIR spectroscopy can provide data with a sufficient signal:noise ratio for identification of specific redox-induced atomic changes in large membrane proteins such as mammalian cytochrome bc_1 complex. The wide range of possible perfusants makes it possible to separate specific components of complex systems, and the ability to record synchronous visible band changes in the same sample provides a means of definitive association of specific IR features with individual redox components. By comparison with model compounds and proteins and by comparison with literature information about related proteins, preliminary assignments of several features of IR difference spectra are possible.

Absolute Spectra and Sample Deposition. Once an aqueous suspension of protein is placed on the prism surface, the 1637 cm^{-1} band of water dominates the absolute spectrum (Figure 1, trace A), due to the fact that it is predominantly water that occupies the small volume above the prism surface that interacts with the evanescent wave of the IR beam. After the sample is dried, however, the spectrum (Figure 1, trace B) becomes dominated instead by the absorption spectrum of protein complexes that form a thin layer on the prism surface. Regardless of the length of the drying process, it is clear from their absolute IR spectra that the dried samples

retain significant amounts of tightly bound water that is never removed (most easily seen in the 3000−4000 cm^{-1} region, not shown). It is likely that this water helps maintain the native structure of the protein during the drying and/or rewetting procedure. The 1649 and 1540 cm^{-1} bands in the dried film arise predominantly from the amide I/II vibrations, and their shapes (*49*) reflect the predominance of α-helical secondary structure. The bands at lower frequencies arise from the plethora of overlapping bands of amino acids and prosthetic groups. The overall shape of the 1700−1200 cm^{-1} region is very consistent between preparations. The band at 1740 cm^{-1} is more variable in relative magnitude, however. It arises from ester carbonyls of the associated phospholipid and is accompanied by a 3010 cm^{-1} band arising from sp^2 hybridized carbon−hydrogen bonds of unsaturated phospholipid (*50*). Hence, the magnitude of these phospholipid bands relative to the protein amide I/II bands may be used as a simple measure of the lipid:protein ratio of the preparations.

Once the sample is rewetted (Figure 1, trace C), the magnitudes of the bands due to protein and lipid decrease uniformly and the water contribution at 1637 cm^{-1} increases as the protein layer swells as it absorbs water. In samples in which detergent depletion is thorough, the sample stabilizes with roughly 50% of the protein absorption bands remaining in the rewetted state.

Overall Reduced minus Oxidized Spectrum. The stability of the rewetted protein film to subsequent changes in perfusant allows redox difference spectra to be recorded with a relatively high signal:noise ratio, and these spectra reveal a range of previously unreported features. In the overall reduced *minus* oxidized difference spectrum shown as Figure 3E, positive peaks are associated with the reduced protein whereas negative peaks will be those of the oxidized form. This is the first reported full IR redox difference spectrum of a cytochrome bc_1 complex. The principle features of the redox spectrum are consistent with those observed in an equivalent spectrum derived from a solubilized sample by transmission FTIR (Figure 3F). This transmission spectrum has a much poorer signal:noise ratio, especially at lower frequencies where the ATR spectrum is enhanced due to the increased depth of penetration of the IR beam (*33*). Nevertheless, the similarity of the major reliable features of this spectrum provides evidence that the protein samples used for ATR are not damaged by the manipulations, a result supported by the fact that the visible spectra of the three heme components remain constant throughout the measurements and are identical to the spectra from the fresh enzyme (Figure 2). This is consistent with prior studies of cytochrome oxidase where IR spectra of CO photolysis were found to be comparable in ATR and transmission samples (*37*).

Changes in the 1700−1610 (in both H_2O and D_2O) and 1570−1500 (in D_2O) cm^{-1} regions will be dominated by changes in the amide I and amide II bands, respectively, and will tend to obscure more informative bands. However, some other features can be assigned tentatively to vibrational changes in amino acid residues, the peptide backbone, and specific redox cofactors (*51*). Specifically, the positive bands at 1406, 1338, and 1238 cm^{-1} (whose positions are relatively unaffected by H−D exchange), together with at least part of the positive bands in the 1550−1530 cm^{-1} region which remains in the D_2O spectrum of Figure 3, are similar to heme modes seen in the redox spectrum of the model compound iron protoporphyrin IX-bisimidazole (*31*) and so might be expected to be associated with cytochrome *b* hemes and, possibly, cytochrome c_1 since the redox spectrum of the "model" cytochrome c_1 subfragment also exhibits some related features (Figure 4, trace D). The 1741 cm^{-1} trough and the 1724 cm^{-1} peak (at least part of which shifts down by several wavenumbers in D_2O) most likely arise from the C═O stretching mode of protonated aspartic and/or glutamic acids (*52*) that have redox-linked perturbations. Unfortunately, the most prominent redox-sensitive ring modes of ubiquinone at 1649 and 1610 cm^{-1} (*53*, *54*) will be obscured by amide I band changes. However, redox-sensitive bands at 1289 and 1264 cm^{-1} that should be relatively insensitive to H−D exchange and have been attributed to methoxy and/or ring modes of ubiquinone (*53*) are in a less crowded region. Hence, troughs at 1289 and 1258 cm^{-1} in the redox spectra of traces E (H_2O) and F (in D_2O) of Figures 3 might be associated with the ubiquinone that is associated with the complex. To assess further such possible assignments, the IR signatures associated with redox changes of specific cofactors were analyzed in more detail below.

Tentative Band Assignments for Cytochrome c_1 and ISP. The use of selective reductants allowed the clean separation of FTIR features associated with redox transitions of cytochrome c_1/ISP, cytochrome b_H/Q_i, and cytochrome b_L. This previously was achieved for the bacterial complex by a combination of spectroelectrochemistry with global deconvolution algorithms (*32*). In the case presented here, such deconvolution was not necessary since the visible spectra (Figure 2) show that redox changes of the three-component hemes have been achieved separately. As a result, and because of the nature of the ATR-FTIR method itself, the signal:noise ratio of these data is greatly improved, even although the bovine enzyme has a larger molecular mass than the bacterial counterpart.

The cytochrome c_1/ISP reduced *minus* oxidized FTIR difference spectrum is shown in Figure 4A. Some assignments as heme C bands can be suggested by comparison with iron-protoporphyrin IX-bisimidazole (*31*), and also with the assignments previously made for the homologous bacterial components (*32*). Comparison with horse heart cytochrome *c* as a model *c*-type cytochrome (*23*), however, proved to be of limited use, despite the fact that both cytochromes *c* and c_1 are type I *c*-type cytochromes and both have His-Met heme coordination (*8*). As a result, a cytochrome c_1-containing subfragment of bovine cytochrome bc_1 complex was isolated (*47*) and its redox IR spectrum was determined so that it could be used as a model template instead (Figure 4D). Comparison of the Figure 4A spectrum with these models suggests heme C features could include the positive bands at 1534, 1516, 1407, 1267, and 1241 cm^{-1} since similar bands appear in the spectra of cytochrome c_1 subfragment (Figure 4D) and/or iron-protoporphyrin IX-bisimidazole (*31*). Similar assignments were made for equivalents of several of these bands in the bacterial cytochrome bc_1 complex (*32*).

Because of the heavier masses of its component atoms, the iron−sulfur prosthetic group of the ISP is not expected to have contributions in the 2000−1000 cm^{-1} region, and only surrounding protein should contribute to redox-induced IR changes. The changes in the 1690−1610 and 1570−1500

Table 2: Peak Positions[a] and Tentative Band Assignments for IR Redox Difference Spectra of Cytochrome c_1/ISP

bovine		*Rb. capsulatus*[b]		model compound		
cyt c_1/ISP[c]	cyt c_1 subcomplex[d]	cyt c_1	ISP	$FePP(Im)_2$[e]	$FePP(Im)_2$[e]	assignment
1691 (−)			1692 (−)			amide I ISP[b]
1657 (−)		1654 (−)	1656 (−)			amide I[b]
1631 (+)	1631 (+)		1632 (−)			amide I[b]
1623 (−)	1622 (−)					amide I[b]
1610 (+)	1612 (+)	1612 (+)	1612 (+)	1616 (+)	1613 (+)	CαCβ heme[e] and amide I ISP[b]
	1558 (+)	1554 (+)		1552 (+)	1553 (+)	CaCm or CbCb heme[b,e]
1534 (+)	1535 (+)	1536 (+)	1532 (+)		1535 (+)	CbCb heme[b,e] and amide II ISP[b]
1516 (+)		1514 (+)				amide II heme[b]
1507 (−)			1504 (−)			amide II ISP[b]
1484 (−)				1481 (−)	1478 (−)	CaCm heme[e]
1464 (+)			1462 (+)			ring of Pro ISP[b]
1446 (−)			1446 (−)			ring of Pro ISP[b]
1407 (+)	1409 (+)	1402 (+)		1405 (+)	1405 (+)	CaN heme[b,e]
1342 (+)				1337 (+)	1337 (+)	CaN or $=CH_2$ vinyl heme[e]
1241 (+)	1243 (+)	1240 (+)		1239 (+)	1239 (+)	CmH heme[b,e]
1214 (+)	1217 (+)			1224 (+)	1224 (+)	CmH heme[e]

[a] Peak positions in the reduced *minus* oxidized spectra are given in cm^{-1}. [b] From Baymann et al. (*32*). [c] From Figure 4A. [d] From Figure 4D. [e] From the spectrum of Fe-protoporphyrin IX-bisimidazole [$FePP(Im)_2$] from Berthomieu et al. (*31*).

Table 3: Peak Positions[a] and Tentative Band Assignments for IR Redox Difference Spectra of Cytochromes b_H and b_L and Ubiquinone

cyt b_L		cyt b_H/Q_i		
bovine[b]	*Rb. capsulatus*[c]	bovine[d]	*Rb. capsulatus*[c]	assignment
1741 (−)		1744 (−)		C=O Asp/Glu
1728 (+)	1720 (+)	1721 (+)	1720 (+)	C=O Asp/Glu[c]
1717 (−)				C=O Asp/Glu
1701 (+)	1704 (+)		1702 (+)	C=O Asp/Glu[c]
1692 (−)	1690 (−)	1688 (−)	1686 (−)	C=O heme propionate[e]
1683 (+)	1680 (+)	1679 (+)	1676 (+)	C=O heme propionate[e]
1675 (−)	1674 (−)			C=O heme propionate[e]
1664 (+)		1665 (+)	1662 (+)	amide I[c]
1649 (−)	1646 (−)	1637 (+)	1642 (+)	amide I[c]
		1656 (−)	1666 (−), 1650(−)	amide I and C=O ubiquinone[c,f]
1612 (+)	1608 (+)	1619 (+)		CαCβ heme[c,g]
		1553 (+)	1554 (+)	CaCm or CbCb heme[c,g]
1549 (−)	1556 (−)			amide II[c]
1537 (+)	1532 (+)	1537 (+)	1534 (+)	CbCb heme[g]
1525 (+)				CbCb heme[g] or amide II
		1486 (+)	1488 (+)	C−C ubisemiquinone ring[c,f]
1407 (+)	1400 (+)	1406 (+)		CaN heme[c,g]
1336 (+)				CaN or $=CH_2$ vinyl heme[g]
		1261 (−)	1262 (−)	OCH_3/ring ubiquinone[c,f]
1237 (+)	1236 (+)	1237 (+)	1236 (+)	CmH heme[c,g]
		1218 (+)		CmH heme[g]

[a] Peak positions in the reduced *minus* oxidized spectra are given in cm^{-1}. [b] From Figure 4B. [c] From Baymann et al. (*32*). [d] From Figure 4C. [e] From Behr et al. (*57*). [f] From Bauscher and Mäntele (*59*) and Hellwig et al. (*60*). [g] From Berthomieu et al. (*31*).

cm^{-1} regions will therefore arise largely from amide I and II changes from both cytochrome c_1 and the ISP and cannot be separated with the present information. However, the very deep trough at 1691 cm^{-1} has previously been associated with the ISP in the *Rhodobacter capsulatus* enzyme (*32*), and is not seen in the cytochrome c_1 subfragment. Hence, it seems likely that this trough is ISP-associated. This frequency can be associated with amide I bonds in turns and bends in the secondary structure (*55*, *56*), and hence, the trough at 1691 cm^{-1} could reflect the conformational change of the flexible hinge region that has been observed by X-ray crystallography to connect the C-terminal domain of the ISP protein to its transmembrane helix (*6*−*8*). Features equivalent to the 1464 cm^{-1} peak and the 1446 cm^{-1} trough in Figure 4A were also assigned tentatively to proline in the ISP (*32*), Further work will be needed to separate and assign in more detail these cytochrome c_1 and ISP signals. The tentative assignments of IR bands for cytochrome c_1 and ISP are summarized in Table 2.

Tentative Band Assignments for Hemes b_H, cyt b_L, and Q_i. Reduced *minus* oxidized FTIR difference spectra of hemes b_L and b_H are shown in Figure 4, and again, some heme band assignments (Table 2) can be made by comparison with spectra of iron-protoporphyrin IX-bisimidazole (*31*) and with the assignments previously made for the homologous bacterial components (*32*). These include bands at 1612 (+), 1407 (+), 1336 (+), and 1237 (+) cm^{-1} in the heme b_L^-/b_L spectrum, and 1619 (+), 1553 (+), 1406 (+), 1237 (+), and 1218 (+) cm^{-1} in the heme b_H^-/b_H spectrum. Assignments to specific heme modes based on assignments in ref *31* are summarized in Table 2. It may be noted that positive bands at 1405−1407 and 1237−1240 cm^{-1} appear to be common to protein-bound and model heme groups, as might be expected for internal vibrational modes of the heme macrocycle. These bands therefore can provide useful general marker bands for heme redox transitions.

The troughs at 1692 cm^{-1} in heme b_L^-/b_L and 1688 cm^{-1} in heme b_H^-/b_H are likely to have contributions from heme

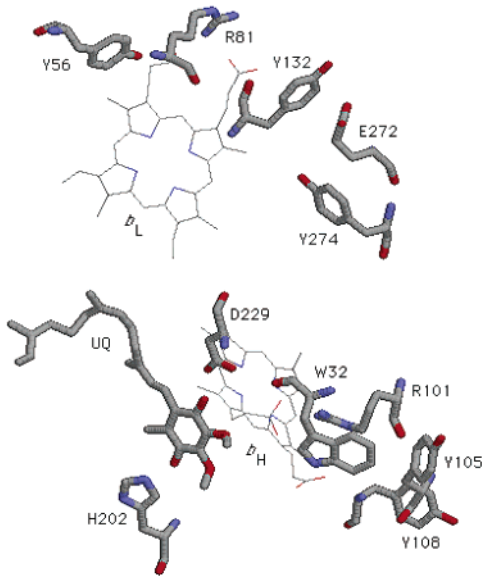

FIGURE 5: Crystallographic data on hemes b_L and b_H and surrounding residues in cytochrome bc_1 complex. Coordinates of chicken cytochrome bc_1 complex were taken from PDB entry 1BCC (*7*) as this contains a crystallographically defined ubiquinone bound at the Q_i site. This figure, drawn using RasMol, shows hemes b_L and b_H together with ubiquinone bound in the Q_i site. Also illustrated are Asp, Glu, His, Arg, Tyr, and Trp residues that are within 8 Å of the surface of one or more of these cofactors in both bovine and chicken structures (chicken numbering).

propionic acid groups (*57*). However, for both heme spectra, the 1700−1610 cm^{-1} region will have contributions from amide I changes while the 1570−1500 cm^{-1} region will contain amide II changes. These protein backbone bands will overlap any underlying heme or specific amino acid bands and are distinct for the two different heme spectra. However, one amino acid region not obscured by the amide I/II bands is that around 1740 cm^{-1} where protonated carboxylic acid residues absorb (*52*). Bands occur in this region at 1741 (−)/1728 (+) and 1717 (−)/1701 (+) cm^{-1} in heme b_{L-}/b_L, and at 1744 (−)/1721 (+) cm^{-1} in heme b_{H-}/b_H, and features in this region were also reported for the bacterial enzyme (*32*). These are likely to represent perturbations and/or protonation and deprotonations of aspartic or glutamic acid residues close to each heme group. Scrutiny of the crystallographic data (*6*−*9*) indicates two plausible candidates for these signals: D229 and E272, associated with the Q_i and Q_o sites, respectively. Of the acidic residues within bovine mitochondrial cyt *b*, only the equivalents of D229 and E272 fall within a 8 Å radius of either heme moiety (see Figure 5). The side chain carboxylate of D229 is oriented toward the pyrrole B propionate carboxylate of heme b_H. The 7 Å separation between these two groups is too large to allow for hydrogen bonding, although long-range electrostatic or conformational interactions may occur. In addition, the carboxylic group of D229 is closely associated with quinone bound at the Q_i site, and is involved in hydrogen bonding via an intermediary water molecule to the headgroup C1 carbonyl of the quinone molecule in the yeast bc_1 structure (*9*). Hence, its perturbation may well be linked instead to redox changes of the Q_i quinone rather than the heme group. E272 forms part of the highly conserved and catalytically essential "PEWY" element of the Q_o site (*58*). The side chain carboxylic acid of E272 is separated by 6.5 Å from the propionic oxygen atoms of heme b_L pyrrole ring A and so may well be influenced by a redox state change of this heme group.

A ubiquinone is retained in this bc_1 complex preparation during protein purification. Quantitation indicates that ubiquinone is present at roughly one per monomeric unit, and it is evident that this quinone resides in the Q_i site. This bound quinone has a relatively stabilized semiquinone, the detailed parameters of which are known (*48*). Several prominent IR bands are lost when free ubiquinone is reduced to either semiquinone or quinol (*53*, *54*, *59*, *60*). Most prominent are the 1649 cm^{-1} bands (C═O) and 1610 cm^{-1} bands (C═C), but these are in the crowded amide I region and are likely to be obscured by other overlapping bands. Combination methoxy/ring vibrations of ubiquinone occur at 1289, 1264, and 1205 cm^{-1} (*53*, *54*, *59*, *60*) and should be less obscured by other signals. Interestingly, the heme b_H spectrum exhibits a trough at 1261 cm^{-1} (Figure 4C). Hence, the 1261 cm^{-1} trough could arise from the reduction of the Q_i site ubiquinone. A similar trough was described and assigned to ubiquinone in a study of the bacterial enzyme (*32*), although in this case the size of the signals relative to the heme bands was very much greater, suggesting that a significant level of "free" ubiquinone might also have copurified with the enzyme. Weaker positive bands due to ubiquinol are known to occur at 1490, 1471, 1431, and 1389 cm^{-1} (*53*, *54*, *59*, *60*), evidence for which was found in studies of the bacterial bc_1 complex (*32*). However, the small size of the troughs that might be due to ubiquinone in the bovine enzyme means that any positive ubiquinol bands would also be extremely small. The spectrum of heme b_H does, however, exhibit a prominent positive peak at 1486 cm^{-1} in this region. Studies with isotopically labeled ubiquinones in the Q_A and Q_B sites in the bacterial reaction center have associated similar large bands with ubisemiquinone (*61*, *62*), as have model compound studies (*54*), and hence, this band in the bovine enzyme might arise from a semiquinone form of ubiquinone in the Q_i site. Equivalent isotope replacement studies on the cytochrome bc_1 complex, together with comparison with spectra for the enzyme in which specific inhibitors have displaced ubiquinone from its binding sites, should provide a means of clarification of the nature of these possible ubiquinone signals.

In summary, this report documents the basic IR redox difference spectra of the major components of the bovine mitochondrial bc_1 complex at a resolution that extends the initial equivalent studies of a bacterial homologue (*32*). Comparison with this previous study, together with comparisons with model materials, has already allowed tentative assignments of many bands. This work is now being extended by enlargement of the model database and by more detailed investigation of the quinone binding sites by use of specific inhibitors and isotopically labelled quinone replacements. Further extension is also underway (in collaboration with P. L. Dutton et al.) for the study of well-defined redox-active maquettes and site-directed mutants of the homologous complex of *Rhodobacter capsulatus*, hence opening the possibility of study by IR spectroscopy of a range of structure and mechanism questions in this class of enzymes that have to date remained unresolved.

ACKNOWLEDGMENT

We are grateful to Dr. Bill Rutherford (CEA-Saclay) for helpful discussions, to Mr. Jonathan Ramsey for expert biochemical technical support, and to Mr. Santiago Garcia for specialist electronic and mechanical support.

REFERENCES

1. Schägger, H., Link, T. A., Engel, W. D., and von Jagow, G. (1986) Isolation of the eleven protein subunits of the *bc*1 complex from beef heart, *Methods Enzymol. 126*, 224−237.
2. Robertson, D. E., Ding, H., Chelminski, P. R., Slaughter, C., Hsu, J., Moomaw, C., Tokito, M., Daldal, F., and Dutton, P. L. (1993) Hydroubiquinone-cytochrome c_2 oxidoreductase from *Rhodobacter capsulatus*: Definition of a minimal, functional isolated preparation, *Biochemistry 32*, 1310−1317.
3. Hosokawa, Y., Suzuki, H., Toda, H., Nishikimi, M., and Ozawa, T. (1990) The primary structure of the precursor to core protein II, a putative member of mitochondrial processing protease family, of rat mitochondrial cytochrome *bc*1 complex deduced from cDNA sequence analysis, *Biochem. Int. 20*, 731−737.
4. Gencic, S., Schägger, H., and von Jagow, G. (1991) Core I protein of bovine ubiquinol-cytochrome-*c* reductase; An additional member of the mitochondrial-protein-processing family: Cloning of bovine core I and core II cDNAs and primary structure of the proteins, *Eur. J. Biochem. 199*, 123−131.
5. Glaser, E., Eriksson, A., and Sjöling, S. (1994) Bifunctional role of the *bc*1 complex in plants: mitochondrial *bc*1 complex catalyses both electron transport and protein processing, *FEBS Lett. 346*, 83−87.
6. Xia, D., Yu, C.-A., Hoeon, K., Xia, J. Z., Kachurin, A. M., Zhang, L., and Deisenhofer, J. (1997) Crystal structure of the cytochrome bc_1 complex from bovine heart mitochondria, *Science 277*, 60−66.
7. Zhang, Z., Huang, L., Shulmeister, V. M., Chi, Y.-I., Kim, K. K., Hung, L.-W., Crofts, A. R., Berry, E. A., and Kim, S.-H. (1998) Electron transfer by domain movement in cytochrome bc_1, *Nature 392*, 677−684.
8. Iwata, S., Lee, J. W., Okada, K., Lee, J. K., Iwata, M., Rasmussen, B., Link, T. A., Ramaswamy, S., and Jap, B. K. (1998) Complete structure of the 11-subunit bovine mitochondrial bc_1 complex, *Science 281*, 64−71.
9. Hunte, C., Koepke, J., Lange, C., Rossmanith, T., and Michel, H. (2000) Structure at 2.3 Å resolution of the cytochrome bc_1 complex from the yeast *Saccharomyces cerevisiae* co-crystallized with an antibody Fv fragment, *Structure 8*, 669−684.
10. Berry, E. A., Guergova-Kuras, M., Huang, L.-S., and Crofts, A. R. (2000) Structure and Function of Cytochrome bc complexes, *Annu. Rev. Biochem. 69*, 1005−1075.
11. Mitchell, P. (1976) Possible molecular mechanisms of the protonmotive function of cytochrome systems, *J. Theor. Biol. 62*, 327−367.
12. Crofts, A. R., Barquera, B., Gennis, R. B., Kuras, R., Guergova-Kuras, M., and Berry, E. A. (1999) Mechanism of Ubiquinol Oxidation by the bc_1 Complex: Different Domains of the Quinol Binding Pocket and Their Role in the Mechanism and Binding of Inhibitors, *Biochemistry 38*, 15807−15826.
13. Jünemann, S., Heathcote, P., and Rich, P. R. (1998) On the mechanism of quinol oxidation in the bc_1 complex, *J. Biol. Chem. 273*, 21603−21607.
14. Darrouzet, E., Moser, C. C., Dutton, P. L., and Daldal, F. (2001) Large scale domain movement in cytochrome bc_1: a new device for electron transfer in proteins, *Trends Biochem. Sci. 26*, 445−451.
15. Crofts, A. R., Guergova-Kuras, M., Huang, L.-S., Kuras, R., Zhang, Z., and Berry, E. A. (1999) Mechanism of ubiquinol oxidation by the bc_1 complex: role of the iron sulfur protein and its mobility, *Biochemistry 38*, 15791−15806.
16. Crofts, A. R., Hong, S., Zhang, Z., and Berry, E. A. (1999) Physiochemical Aspects of the Movement of the Rieske Iron Sulfur Protein during Quinol Oxidation by the bc_1 Complex from Mitochondria and Photosynthetic Bacteria, *Biochemistry 38*, 15827−15839.
17. Ding, H., Robertson, D. E., Daldal, F., and Dutton, P. L. (1992) Cytochrome bc_1 complex [2Fe-2S] cluster and its interaction with ubiquinone and ubihydroquinone at the Q_o site: A double-occupancy Q_o site model, *Biochemistry 31*, 3144−3158.
18. Brandt, U., Schägger, H., and von Jagow, G. (1988) Characterisation of binding of the methoxyacrylate inhibitors to mitochondrial cytochrome *c* reductase, *Eur. J. Biochem. 173*, 499−506.
19. Bartoschek, S., Johansson, M., Geierstanger, B. H., Okun, J. G., Lancaster, C. R. D., Humpfer, E., Yu, L., Yu, C.-A., Griesinger, C., and Brandt, U. (2001) Three molecules of ubiquinone bind specifically to mitochondrial cytochrome bc1 complex, *J. Biol. Chem. 276*, 35231−35234.
20. Brandt, U. (1996) Bifurcated ubihydroquinone-oxidation in the cytochrome bc_1 complex by proton-gated charge-transfer, *FEBS Lett. 387*, 1−6.
21. Mäntele, W., Nabedryk, E., Tavitian, B. A., Kreutz, W., and Breton, J. (1985) Light-induced Fourier transform infrared (FTIR) spectroscopic investigations of the primary oxidation in bacterial photosynthesis, *FEBS Lett. 187*, 227−232.
22. Tabitian, B. A., Nabedryk, E., Mantele, W., and Breton, J. (1986) Light-induced Fourier transform infrared (FTIR) spectroscopic investigations of primary reactions in photosystem I and photosystem II, *FEBS Lett. 201*, 151−157.
23. Moss, D., Nabedryk, E., Breton, J., and Mäntele, W. (1990) Redox-linked conformational changes in proteins detected by a combination of IR spectroscopy and protein electrochemistry. Evaluation of the technique with cytochrome *c*, *Eur. J. Biochem. 187*, 565−572.
24. Hellwig, P., Rost, B., Kaiser, U., Ostermeier, C., Michel, H., and Mäntele, W. (1996) Carboxyl group protonation upon reduction of the *Paracoccus denitrificans* cytochrome *c* oxidase: Direct evidence by FTIR spectroscopy, *FEBS Lett. 385*, 53−57.
25. Hellwig, P., Behr, J., Ostermeier, C., Richter, O.-M. H., Pfitzner, U., Odenwald, A., Ludwig, B., Michel, H., and Mäntele, W. (1998) Involvement of glutamic acid 278 in the redox reaction of the cytochrome *c* oxidase from *Paracoccus denitrificans* investigated by FTIR spectroscopy, *Biochemistry 37*, 7390−7399.
26. Lübben, M., and Gerwert, K. (1996) Redox FTIR difference spectroscopy using caged electrons reveals contributions of carboxyl groups to the catalytic mechanism of haem-copper oxidases, *FEBS Lett. 397*, 303−307.
27. Yamazaki, Y., Kandori, H., and Mogi, T. (1999) Effects of subunit I mutations on redox-linked conformational changes of the *Escherichia coli* bo-type ubiquinol oxidase revealed by Fourier transform infrared spectroscopy, *J. Biochem. 126*, 194−199.
28. Lübben, M., Prutsch, A., Mamat, B., and Gerwert, K. (1999) Electron-transfer induces side-chain conformational changes of glutamate-286 from cytochrome bo_3, *Biochemistry 38*, 2048−2056.
29. Hellwig, P., Soulimane, T., Buse, G., and Mäntele, W. (1999) Similarities and dissimilarities in the structure−function relation between the cytochrome *c* oxidase from bovine heart and from *Paracoccus denitrificans* as revealed by FT-IR difference spectroscopy, *FEBS Lett. 458*, 83−86.
30. Hellwig, P., Scheide, D., Bungert, S., Mäntele, W., and Friedrich, T. (2000) FT-IR spectroscopic characterization of NADH:ubiquinone oxidoreductase (complex I) from *Escherichia coli*: oxidation of FeS cluster N2 is coupled with the protonation of an aspartate or glutamate side chain, *Biochemistry 39*, 10884−10891.
31. Berthomieu, C., Boussac, A., Mäntele, W., Breton, J., and Nabedryk, E. (1992) Molecular changes following oxidoreduction of cytochrome *b*559 characterized by Fourier transform infrared difference spectroscopy and electron paramagnetic resonance: Photooxidation in photosystem II and electrochemistry of isolated cytochrome *b*559 and iron protoporphyrin IX-bisimidazole model compounds, *Biochemistry 31*, 11460−11471.
32. Baymann, F., Robertson, D. E., Dutton, P. L., and Mäntele, W. (1999) Electrochemical and spectroscopic investigations of the cytochrome bc_1 complex from *Rhodobacter capsulatus*, *Biochemistry 38*, 13188−13199.
33. Goormaghtigh, E., Raussens, V., and Ruysschaert, J.-M. (1999) Attenuated total reflection infrared spectroscopy of proteins and lipids in biological membranes, *Biochim. Biophys. Acta 1422*, 105−185.
34. Heberle, J., and Zscherp, C. (1996) ATR/FT-IR difference spectroscopy of biological matter with microsecond time resolution, *Appl. Spectrosc. 50*, 588−596.
35. Zscherp, C., Schlesinger, R., Tittor, J., Oesterhelt, D., and Heberle, J. (1999) In situ determinatin of transient pK_a changes of internal amino acids of bacteriorhodopsin by using time-resolved atenuated total reflection Fourier-transform infrared spectroscopy, *Proc. Natl. Acad. Sci. U.S.A. 96*, 5498−5503.

36. Baenziger, J. E., Miller, K. W., and Rothschild, K. J. (1993) Fourier transform infrared difference spectroscopy of the nicotinic acetylcholine receptor: evidence for specific protein structural changes upon desensitization, *Biochemistry 32*, 5448−5454.
37. Rich, P. R., and Breton, J. (2002) Attenuated total reflection Fourier transform infrared studies of redox changes in bovine cytochrome *c* oxidase: Resolution of the redox Fourier transform infrared difference spectrum of heme a_3, *Biochemistry 41*, 967−973.
38. Nyquist, R. M., Heitbrink, D., Bolwien, C., Wells, T. A., Gennis, R., and Heberle, J. (2001) Perfusion-induced redox differences in cytochrome *c* oxidase: ATR/FT-IR spectroscopy, *FEBS Lett. 505*, 63−67.
39. Iwaki, M., Breton, J., and Rich, P. R. (2002) ATR-FTIR difference spectroscopy of the P_M intermediate of bovine cytochrome *c* oxidase, *Biochim. Biophys. Acta 1555*, 116−121.
40. Iwaki, M., Andrianambinintsoa, S., Rich, P. R., and Breton, J. (2002) Attenuated total reflection Fourier transform infrared spectroscopy of redox transitions in photosynthetic reaction centers: comparison of perfusion- and light-induced difference spectra, *Spectrochim. Acta, Part A 58*, 1523−1533.
41. Hartzell, C. R., Beinert, H., van Gelder, B. F., and King, T. E. (1978) Preparation of cytochrome oxidase from beef heart, *Methods Enzymol. 53*, 54−66.
42. Yu, C. A., Yu, L., and King, T. E. (1974) Soluble cytochrome bc_1 complex and the reconstitution of succinate-cytochrome *c* reductase, *J. Biol. Chem. 249*, 4905−4910.
43. King, T. E. (1978) Cytochrome c_1 from mammalian heart, *Methods Enzymol. 53*, 181−191.
44. Takamiya, K., and Dutton, P. L. (1979) Ubiquinone in *Rhodopseudomonas sphaeroides*. Some thermodynamic properties, *Biochim. Biophys. Acta 546*, 1−16.
45. Glasoe, P. K., and Long, F. A. (1960) Use of glass electrodes to measure acidities in deuterium oxide, *J. Phys. Chem. 64*, 188−190.
46. Rath, P., DeGrip, W. J., and Rothschild, K. J. (1998) Photoactivation of rhodopsin causes an increased hydrogen−deuterium exchange of buried peptide groups, *Biophys. J. 74*, 192−198.
47. Schägger, H., von Jagow, G., Borchart, U., and Machleidt, W. (1983) Amino acid sequence of the smallest protein of the cytochrome c_1 subcomplex from beef heart mitochondria, *Hoppe-Seyler's Z. Physiol. Chem. 364*, 307−311.
48. Rich, P. R., Jeal, A. E., Madgwick, S. A., and Moody, A. J. (1990) Inhibitor effects on the redox-linked protonations of the *b* haems of the mitochondrial bc_1 complex, *Biochim. Biophys. Acta 1018*, 29−40.
49. Arrondo, J. L. R., Muga, A., Castresana, J., and Goñi, F. M. (1993) Quantitative studies of the structure of proteins in solution by Fourier-transform infrared spectroscopy, *Prog. Biophys. Mol. Biol. 59*, 23−56.
50. Stuart, B. (1997) in *Biological Applications of Infrared Spectroscopy*, John Wiley & Sons, Chichester, U.K.
51. Mantele, W. (1996) in *Biophysical Techniques in Photosynthesis* (Amesz, J., and Hoff, A. J., Eds.) pp 137−160, Kluwer Academic Publishers, Dordrecht.
52. Barth, A. (2000) The infrared absorption of amino acid side chains, *Prog. Biophys. Mol. Biol. 74*, 141−173.
53. Burie, J.-R., Boussac, A., Boullais, C., Berger, G., Mattioli, T., Mioskowski, C., Nabedryk, E., and Breton, J. (1995) FTIR spectroscopy of UV-generated quinone radicals: Evidence for an intramolecular hydrogen atom transfer in ubiquinone, naphthoquinone, and plastoquinone, *J. Phys. Chem. 99*, 4059−4070.
54. Bauscher, M., Nabedryk, E., Bagley, K., Breton, J., and Mäntele, W. (1990) Investigation of models for photosynthetic electron acceptors: Infrared spectroelectrochemistry of ubiquinone and its anions, *FEBS Lett. 261*, 191−195.
55. Kalnin, N. N., Baikalov, I. A., and Venyaminov, S. Y. (1990) Quantitative IR spectrophotometry of peptide compounds in water (H_2O) solutions. II. Estimation of the protein secondary structure, *Biopolymers 30*, 1273−1280.
56. Venyaminov, S. Y., and Kalnin, N. N. (1990) Quantitative IR spectrophotometry of peptide compounds in water (H_2O) solutions. Amide II absorption bands of polypeptides and fibrous proteins in α-, *β*-, and random coil conformations, *Biopolymers 30*, 1259−1271.
57. Behr, J., Hellwig, P., Mäntele, W., and Michel, H. (1998) Redox dependent changes at the heme propionates in cytochrome *c* oxidase from *Paracoccus denitrificans*: Direct evidence from FTIR difference spectroscopy in combination with heme propionate ^{13}C labeling, *Biochemistry 37*, 7400−7406.
58. Fisher, N., and Rich, P. R. (2000) A motif for quinone binding sites in respiratory and photosynthetic systems, *J. Mol. Biol. 296*, 1153−1162.
59. Bauscher, M., and Mäntele, W. (1992) Electrochemical and infrared-spectroscopic characterization of redox reactions of p-quinones, *J. Phys. Chem. 96*, 11101−11108.
60. Hellwig, P., Mogi, T., Tomson, F. L., Gennis, R. B., Iwata, J., Miyoshi, H., and Mäntele, W. (1999) Vibrational modes of ubiquinone in cytochrome bo_3 from *Escherichia coli* ientified by Fourier transform infrared difference spectroscopy and specific ^{13}C labeling, *Biochemistry 38*, 14683−14689.
61. Breton, J., Boullais, C., Burie, J.-R., Nabedryk, E., and Mioskowski, C. (1994) Binding sites of quinones in photosynthetic bacterial reaction centers investigated by light-induced FTIR difference spectroscopy: Assignment of the interactions of each carbonyl of Q_A in *Rhodobacter sphaeroides* using site-specific ^{13}C-labeled ubiquinone, *Biochemistry 33*, 14378−14386.
62. Breton, J., Boullais, C., Berger, G., Mioskowski, C., and Nabedryk, E. (1995) Binding sites of quinones in photosynthetic bacterial reaction centers investigated by light-induced FTIR difference spectroscopy: Symmetry of the carbonyl interactions and close equivalence of the Q_B vibrations in *Rhodobacter sphaeroides* and *Rhodopseudomonas viridis* probed by isotope labeling, *Biochemistry 34*, 11606−11616.
63. Rich, P. R. (1983) Electron transfer through the isolated mitochondrial cytochrome $b-c_1$ complex, *Biochim. Biophys. Acta 722*, 271−280.
64. Trumpower, B. L. (1981) Function of the iron−sulfur protein of the cytochrome b−c1 segment in electron-transfer and energy-conserving reactions of the mitochondrial respiratory chain, *Biochim. Biophys. Acta 639*, 129−155.
65. Rich, P. R. (1984) Electron and proton transfers through quinones and cytochrome *bc* complexes, *Biochim. Biophys. Acta 768*, 53−79.

BI0343020